PHYSICAL REVIEW B **88**, 094509 (2013)

Low-temperature phase diagram of $Fe_{1+y}Te$ studied using x-ray diffraction

Cevriye Koz,[1] Sahana Rößler,[1,*] Alexander A. Tsirlin,[1,2] Steffen Wirth,[1] and Ulrich Schwarz[1,†]
[1]*Max Planck Institute for Chemical Physics of Solids, Nöthnitzer Straße 40, 01187 Dresden, Germany*
[2]*National Institute of Chemical Physics and Biophysics, 12618 Tallinn, Estonia*

(Received 12 July 2013; revised manuscript received 5 September 2013; published 18 September 2013)

We used low-temperature synchrotron x-ray diffraction to investigate the structural phase transitions of $Fe_{1+y}Te$ in the vicinity of a tricitical point in the phase diagram. A detailed analysis of the powder diffraction patterns and temperature dependence of the peak widths in $Fe_{1+y}Te$ showed that two-step structural and magnetic phase transitions occur within the compositional range $0.11 \leqslant y \leqslant 0.13$. The phase transitions are sluggish, indicating a strong competition between the orthorhombic and the monoclinic phases. We combine high-resolution diffraction experiments with specific heat, resistivity, and magnetization measurements and present a revised temperature-composition phase diagram for $Fe_{1+y}Te$.

DOI: 10.1103/PhysRevB.88.094509 PACS number(s): 74.70.Xa, 74.62.Bf

I. INTRODUCTION

Iron chalcogenides, Fe_{1+y}(Te,Se), are promising candidates to understand the mechanism of superconductivity in the family of Fe-based superconductors owing to their archetypical binary atomic pattern. The tetragonal PbO-type $Fe_{1+y}Se$ with a superconducting transition temperature $T_c = 8$ K is the simplest member of Fe-based superconductors because of its structure and chemical composition.[1] The structure comprises stacks of edge-sharing $FeSe_4$ tetrahedra, which form layers orthogonal to the c axis. The homogeneity range of tetragonal $Fe_{1+y}Se$ is very narrow. The compound is nearly stoichiometric, and a minute change in the composition controls the physical and low-temperature structural properties. For example, $Fe_{1.01}Se$ is superconducting and the crystal structure transforms from a tetragonal ($P4/nmm$) to an orthorhombic ($Cmma$) phase at around 90 K, whereas nonsuperconducting $Fe_{1.03}Se$ does not exhibit this structural transition.[2] The T_c of $Fe_{1+y}Se$ can be enhanced up to 37 K by applying an external pressure of 7–9 GPa,[3–5] or up to 15 K by about 50% substitution of Te at ambient pressure.[6–8] The bulk superconductivity disappears with higher Te substitution and the end member, $Fe_{1+y}Te$, is nonsuperconducting.

$Fe_{1+y}Te$ with an analogous crystal structure to $Fe_{1+y}Se$ occurs only in the presence of excess Fe, which is situated in the interstitial $2c$ crystallographic sites within the chalcogenide planes.[9] Instead of superconductivity, tetragonal $Fe_{1+y}Te$ shows a complex interplay of magnetic and structural phase transitions in dependence on the excess amount of Fe.[9–14] A simultaneous first-order magnetic and structural transition from the tetragonal paramagnetic to the monoclinic ($P2_1/m$) commensurate antiferromagnetic phase is observed at $T = 69$ K in $Fe_{1.06}Te$. The first-order transition temperature systematically decreases down to 57 K with an increase in y from 0.06 to 0.11. For $y > 0.11$, two transitions are observed: in the specific case of $y = 0.13$, a continuous transition at 57 K and a first-order phase transition at lower temperature. This behavior suggests the presence of a tricritical point close to this composition. For larger amounts of interstitial Fe, $y = 0.15$, once again a single phase transition is observed at 63 K in the heat capacity measurements. However, this phase transition is a continuous[14] (λ-like in specific heat) transition from a tetragonal paramagnetic to orthorhombic incommensurate antiferromagnetic phase.[9,12] The microscopic mechanisms driving these phase transitions are not yet well understood.

A strong influence of excess Fe on the magnetic and crystallographic properties of $Fe_{1+y}Te$ ($y = 0.076$, 0.141, and 0.165) was first reported by Bao *et al.* based on neutron diffraction experiments.[9] Following this report, several other groups made similar observations.[12–15] However, due to the extreme sensitivity of the physical properties of $Fe_{1+y}Te$ to the amount of y, it is often difficult to compare the results of independent measurements. Furthermore, Rodriguez *et al.* reported a phase diagram[12] of $Fe_{1+y}Te$ for Fe:Te in the nominal range 1.04–1.18:1, while a report by Mizuguchi *et al.* extended the phase diagram[15] up to 1.3:1. These results suggest an ambiguity in the homogeneity range of the room temperature tetragonal phase of $Fe_{1+y}Te$. Therefore, our goal here is to establish the homogeneity range based on careful x-ray diffraction experiments and physical property measurements on chemically well-characterized samples. In our previous study,[14] we presented a tentative phase diagram of $Fe_{1+y}Te$, which is incomplete around the composition $y = 0.11$. In the case of $Fe_{1.13}Te$, we reported two thermodynamic anomalies, and assigned the phase transition at lower temperature $T_s = 46$ K to the structural transformation.[14] However, a recent report[15] on the same nominal composition by Mizuguchi *et al.* shows a two-step structural phase transition, from a tetragonal-orthorhombic followed by an orthorhombic-monoclinic structure upon cooling. Further, the neutron diffraction data on $Fe_{1.10}Te$ with similar thermodynamic properties such as our $Fe_{1.13}Te$ indicated a structural anomaly at 63 K followed by a long-range magnetic order at 57.5 K. These different results may also be related to subtle differences in the Fe content.[13] Here, we focus on the detailed analysis of the powder diffraction patterns and the temperature dependence of the peak width in $Fe_{1+y}Te$ within the range $0.11 \leqslant y \leqslant 0.15$ to understand which phases are involved close to the tricritical point in the $Fe_{1+y}Te$ phase diagram. We aim to fill in the gaps as well as revise the phase diagram to gain a clearer picture of the interplay between structure and magnetism in these compounds.

II. EXPERIMENT

Polycrystalline $Fe_{1+y}Te$ samples were synthesized utilizing the solid-state reaction method as described in Ref. 16 with different amounts of excess iron in the range $0.02 \leqslant y \leqslant 0.20$. Prepared samples were investigated by x-ray powder diffraction (XRD) using Co $K\alpha_1$ radiation ($\lambda = 1.788\,965$ Å). The lattice parameters of the samples were calculated with $\mathrm{LaB_6}$ as an internal standard in the x-ray powder diffraction experiments. As the amount of excess iron is extremely important for the physical properties of $\mathrm{Fe}_{1+y}\mathrm{Te}$, the synthesized phase-pure samples were characterized by wavelength dispersive x-ray (WDX) analysis and the inductively coupled plasma (ICP) method to determine the amount of Fe. For the WDX measurements, FeGe and Te are taken as reference materials for Fe and Te, respectively. In the ICP analysis, for each composition, three different solutions were prepared by dissolving 5–8 mg of samples in aqua regia ($\mathrm{HNO_3}$:HCl in a volume ratio 1:3). The specific heat $C_p(T)$ and electrical resistivity $\rho(T)$ were measured employing a Quantum Design physical property measurement system (PPMS). The magnetic susceptibility $\chi(T)$ was obtained by means of a superconducting quantum interference device (SQUID) magnetometer. The powders of polycrystalline materials for synchrotron measurements were ground from exactly the same pieces that were used for heat capacity, resistivity, and magnetic susceptibility measurements in order to correlate the structural phase transitions with the physical properties at a given composition. The diffraction data were collected on the high-resolution powder diffraction beamline ID31 ($\lambda = 0.430\,46$ Å) at the ESRF, Grenoble, using a special He-flow cryostat adapted to the diffraction setup environment. Lattice parameter determination and structure refinements were performed by the least-squares method using JANA2006.[17] In Rietveld refinement procedures, anisotropic strain broadening and the March-Dollase approach for describing the preferred orientation were applied.[18,19]

III. RESULTS AND DISCUSSION

The XRD patterns of $\mathrm{Fe}_{1+y}\mathrm{Te}$ ($y = 0.04$, 0.06, 0.08, 0.11, 0.13, 0.15, and 0.17) samples at ambient temperature are presented in Fig. 1(a). $\mathrm{FeTe_2}$ and Fe impurities were observed in XRD patterns for compositions $y < 0.06$ and $y > 0.15$, respectively. Previously reported excess amounts of iron in tetragonal $\mathrm{Fe}_{1+y}\mathrm{Te}$ ranged from 0% to 30%.[12,15,20–22] According to our x-ray diffraction study and lattice parameters represented in Figs. 1(a) and 1(b), the homogeneity range of tetragonal $\mathrm{Fe}_{1+y}\mathrm{Te}$ is clearly smaller than those given in these previous reports. For further analysis, only the samples without any detectable traces of $\mathrm{FeTe_2}$ and Fe impurities were considered. In Fig. 2, the experimentally determined composition by the WDX and ICP spectroscopic methods are compared to the nominal composition. In the inset of Fig. 2, a representative backscattered electron (BSE) image of $\mathrm{Fe_{1.13}Te}$ is presented. All investigated samples were similarly single phase, except one, which was consequently excluded from further investigations. The standard deviations for the ICP (WDX) analysis were calculated by averaging over three (ten) independent measurements for each sample, respectively. Here we note that the ICP analysis measures the average composition of the bulk, whereas the WDX is more surface sensitive. While the amount of Fe as obtained by the ICP method is systematically 1%–2% higher than the nominal composition, the WDX analysis gives an amount of iron that is typically 1%–3% lower. The compositions obtained from the WDX and chemical analysis overlap with the nominal composition within three standard deviations, 3σ.

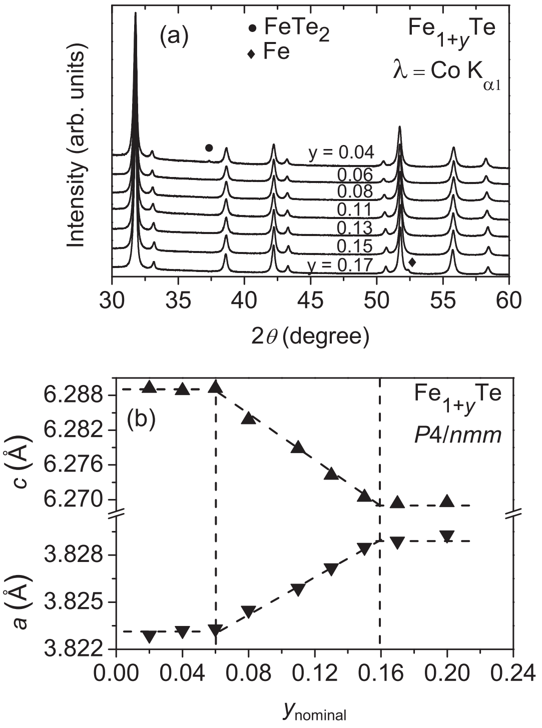

FIG. 1. (a) X-ray diffraction diagram of samples with nominal composition $\mathrm{Fe}_{1+y}\mathrm{Te}$ for $y = 0.04$–0.17, tetragonal $\mathrm{Fe}_{1+y}\mathrm{Te}$ as the main phase at room temperature. (Impurity phases: $\mathrm{FeTe_2}$ marked by filled circle and elemental Fe by ♦.) (b) Lattice parameters at room temperature in dependence of the nominal composition $\mathrm{Fe}_{1+y}\mathrm{Te}$. The error bars here are smaller than the size of the symbols.

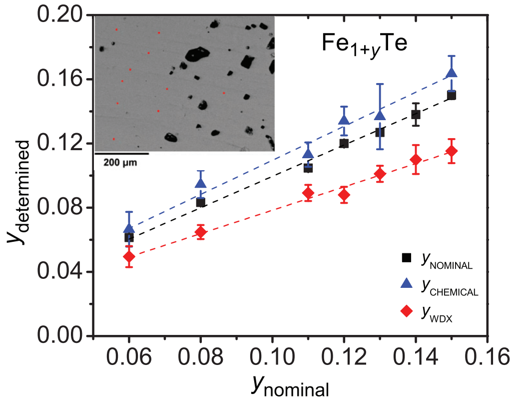

FIG. 2. (Color online) Determined compositions of $\mathrm{Fe}_{1+y}\mathrm{Te}$ with wavelength dispersive x-ray (WDX) analysis and chemical analysis by an inductively coupled plasma method (ICP). In calculating the standard deviation of the nominal compositions, mass loss after reaction was accounted for assuming that all loss is caused by tellurium evaporation. However, this error bar is smaller than the symbol size. The inset shows a representative backscattered electron (BSE) image of $\mathrm{Fe_{1.13}Te}$. The WDX analysis was performed on ten different spots, indicated by red dots on the image. The black spots on the image are pores in the sample.

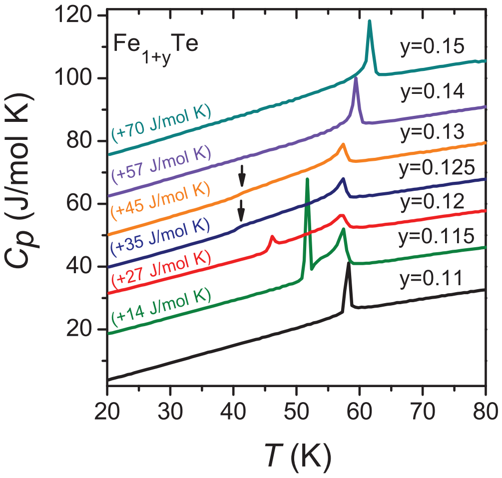

FIG. 3. (Color online) Specific heat of $Fe_{1+y}Te$ for $y = 0.11$–0.15. The $C_p(T)$ data for $y = 0.115$–0.15 are shifted by the amounts given for each curve for clarity. Arrows show the disappearing first-order phase transition upon increasing Fe composition.

The temperature dependence of the specific heat of $Fe_{1+y}Te$ for $y = 0.11$–0.15 is presented in Fig. 3. For $y = 0.11$, a peak corresponding to a simultaneous first-order magnetic and structural phase transition at ≈58 K is observed. With a minute increase in the Fe composition, however, two phase transitions can be distinguished. Already for $y = 0.115$ these two transitions are well separated. For the composition $Fe_{1.12}Te$, the λ-like second-order phase transition at 57 K is followed by a first-order phase transition at lower temperature, 46 K, as reported previously for a single crystal with nominal composition $Fe_{1.13}Te$.[14] With increasing Fe content, the first-order phase transition at lower temperature disappears and for $y = 0.14$ only one transition is detected around 59 K with the characteristics of a continuous phase transition. The corresponding transition for $y = 0.15$ is found at a slightly increased temperature of 63 K.

In order to compare the crystallographic phase transitions of $Fe_{1+y}Te$ compositions to their magnetic and electrical properties, we performed magnetic susceptibility $\chi(T)$ and resistivity $\rho(T)$ measurements. Figures 4(a)–4(e) display the temperature dependence of magnetic susceptibility measured under a magnetic field of 0.1 T in a field-cooling (FC) protocol for $0.11 \leqslant y \leqslant 0.15$. The magnitude of χ rises with increasing y because excess Fe has a strong magnetic moment.[23] The transition temperatures obtained from specific heat and susceptibility measurements are in good agreement. The cooling and warming cycles in the susceptibility measurements exhibit a small thermal hysteresis for $Fe_{1.11}Te$, which is typical for a first-order phase transition [Fig. 4(a)]. This thermal hysteresis in χ is broader for samples with $y = 0.12$ and 0.13 for which specific heat measurements indicated the presence of two consecutive phase transitions. For even higher values of y, cf. Figs. 4(d) and 4(e), there is no thermal hysteresis in magnetic susceptibility measurement. Such behavior is in accordance with what is expected for a continuous phase transition. Figure 4(f) presents a summary of the temperature dependence of normalized resistance ($R/R_{300\,\mathrm{K}}$) measured in the heating cycle. Below the phase transition temperatures, $Fe_{1.11}Te$ shows a metallic behavior, while samples with a higher Fe content, $y \geqslant 0.14$, display increasing resistivity with decreasing temperature. In Fig. 5, resistivity measurements performed in both heating and cooling protocols for $Fe_{1+y}Te$ with $y = 0.11$, 0.12, 0.13, and 0.14 are presented. The

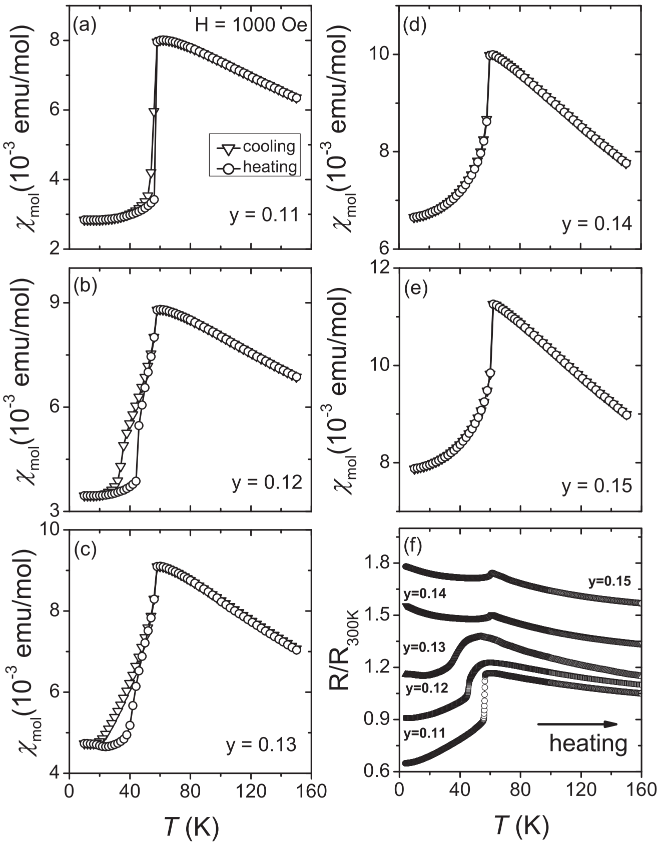

FIG. 4. Magnetic susceptibility of $Fe_{1+y}Te$ for $y = 0.11$–0.15 (a)–(e) and normalized resistance ($R/R_{300\,\mathrm{K}}$) during the heating cycle (f). The magnetic susceptibility was measured in a field of 0.1 T. The $R/R_{300\,\mathrm{K}}$ data for $y = 0.14$ and 0.15 are multiplied by a factor of 1.25 and 1.5, respectively, for better visibility.

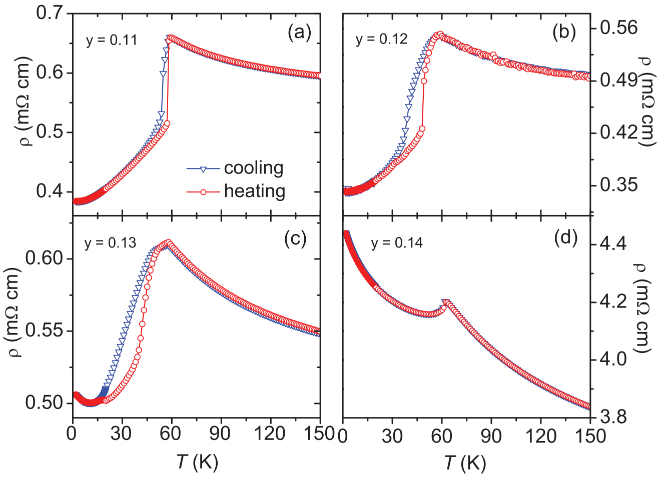

FIG. 5. (Color online) Resistivity as a function of temperature for $Fe_{1+y}Te$ measured in the heating and cooling cycles. (a) $y = 0.11$, (b) $y = 0.12$, (c) $y = 0.13$, and (d) $y = 0.14$.

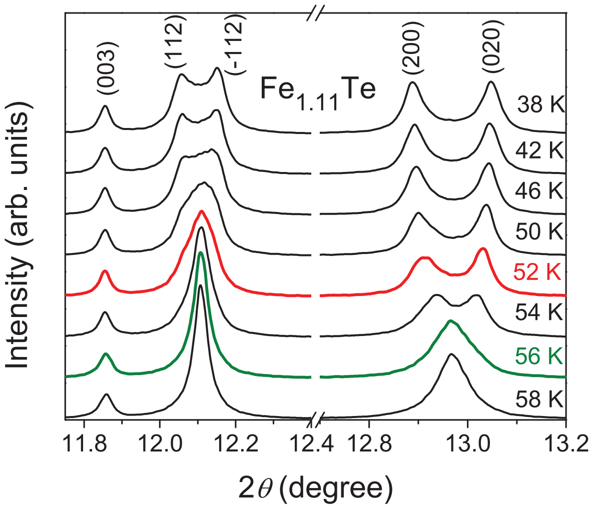

FIG. 6. (Color online) Representative powder XRD patterns of $Fe_{1.11}Te$ in the temperature regime 38–58 K for the (112) and (200) Bragg reflections. The green and red curves indicate an onset of orthorhombic and monoclinic distortions, respectively.

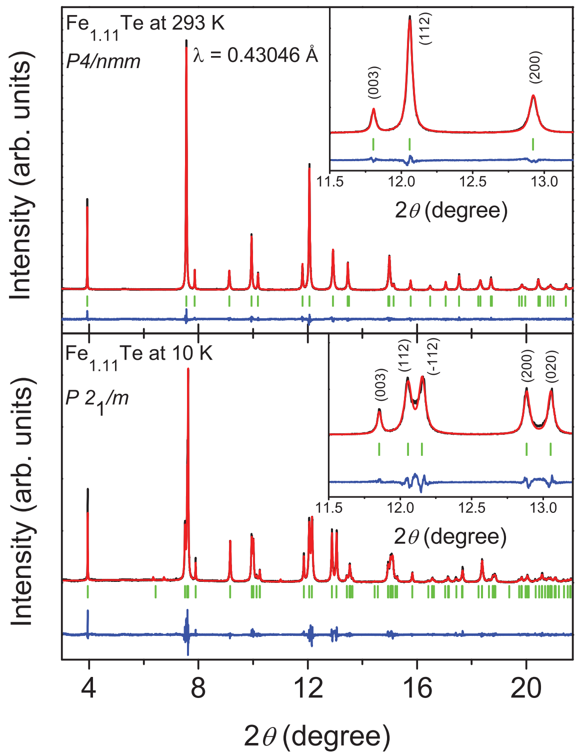

FIG. 7. (Color online) Refined synchrotron powder x-ray diffraction patterns of $Fe_{1.11}Te$ at temperatures above (293 K) and below (10 K) the phase transition.

thermal hysteresis observed for samples with $y = 0.11$, 0.12, and 0.13 in the resistivity measurements [Figs. 5(a)–5(c)] are very similar to those observed in $\chi(T)$ for the same compositions. The absence of thermal hysteresis for sample $y = 0.14$ [Fig. 5(d)] as well as for samples with more Fe excess (not shown) is in accordance with the expectation for a second-order phase transition.

To correlate the physical properties with the crystal structures, we performed high-resolution synchrotron x-ray diffraction of the polycrystalline $Fe_{1+y}Te$ samples for $y =$ 0.11, 0.12, 0.13, 0.14, and 0.15 from 10 to 70 K with 2 K temperature intervals. A complete structure refinement was conducted for all studied compositions. Figure 6 represents the selected region of the XRD pattern for the (112) and (200) Bragg reflections of $Fe_{1.11}Te$ in the temperature regime 38–58 K during the cooling cycle. The peak splitting of both (200) and (112) Bragg reflections is characteristic of the monoclinic ($P2_1/m$) phase transition in the $Fe_{1+y}Te$ system. In Fig. 6, a broadening of the (200) reflection can be seen at 56 K, while the peak splits into (200) and (020) at 54 K. A broadening of the (112) reflection is visible at 52 K and the splitting into (112) and (-112) becomes more pronounced at lower temperatures. A full-profile refinement of powder XRD data of $Fe_{1.11}Te$ at room temperature and 10 K is given in Fig. 7. According to the Rietveld refinement, the composition is determined as $Fe_{1.108(1)}Te$, which is consistent with the nominal composition. The refined data confirm the temperature-induced transformation from tetragonal ($P4/nmm$ at 293 K) to the monoclinic phase ($P2_1/m$ at 10 K) at low temperature. Refined parameters of the crystal structures are represented in Table I. Note that there is no indication for any presence of an orthorhombic phase in $Fe_{1.11}Te$ at 10 K.

In the case of $Fe_{1.12}Te$ with two distinct phase transitions, the broadening of the (200) reflection starts at around 54 K and the splitting is visible at 50 K [Fig. 8(a)]. However, for the (112) peak, no apparent change of the peak shape was observed down to 42 K [see Fig. 8(b)]. Below 42 K, the (112) peak starts broadening, but no clear splitting is observed even at the base temperature, 10 K, in contrast to $Fe_{1.11}Te$. Our observations confirm that $Fe_{1.12}Te$ consists of a mixture of orthorhombic ($Pmmn$) and monoclinic ($P2_1/m$) phases at low temperature, as reported by Rodriguez *et al.*[12] From the results of specific heat and synchrotron XRD measurements, the λ-like second-order phase transition at 57 K is associated with the structural phase transition from tetragonal to orthorhombic symmetry, while the first-order phase transition observed in the specific heat measurements at 46 K corresponds to an orthorhombic to monoclinic phase transition. The latter phase transition in $Fe_{1.12}Te$ is sluggish because of a strong competition between orthorhombic and monoclinic phases. The presence of a phase mixture at low temperatures suggests that there are kinetic barriers to the first-order phase transition with metastable states persisting over long periods of time.

The powder x-ray diffraction patterns of $Fe_{1.12}Te$ and $Fe_{1.13}Te$ at several temperatures were investigated by Rietveld refinement to determine the crystal structure at different temperatures. At 70 K, the XRD pattern can be refined as a single tetragonal phase. At 10 K, the XRD pattern of $Fe_{1.12}Te$ can only be fitted reasonably as a mixture of orthorhombic and monoclinic phases (Fig. 9). However, a substantial overlap of all reflections of the orthorhombic and monoclinic phases makes the refinement of their volume ratio somewhat ambiguous, especially at temperatures right below the transition, where the difference in the lattice parameters of the two phases is very small. At 10 K, the reflections of the two phases are somewhat better separated (see the bottom part of Fig. 9), and we obtain the relative phase fractions (in wt %)

TABLE I. Parameters of crystal structures and refinements, atomic positions, and atomic displacement parameters U_{iso} (in 10^{-2} Å^2) for $\mathrm{Fe}_{1.11}\mathrm{Te}$ at room temperature and 10 K.

Temperature	293 K	10 K
Space group	$P4/nmm$	$P2_1/m$
a (Å)	3.8253(3)	3.83684(8)
b (Å)	$=a$	3.78735(8)
c (Å)	6.27870(6)	6.25409(13)
β (deg)	90	90.668(1)
R_I/R_P	0.015/0.060	0.015/0.089
Number of reflections	81	323
Refined parameters for profile/crystal structure	21/5	30/10
Atomic parameters		
Fe1	$2a\,(\frac{3}{4},\frac{1}{4},0)$	$2e\,(x,\frac{1}{4},z)$
		$x = 0.7368(4)$
		$z = 0.0004(3)$
	$U_{\mathrm{iso}} = 0.83(2)$	$U_{\mathrm{iso}} = 0.68(3)$
Fe2	$2c\,(\frac{1}{4},\frac{1}{4},z)$	$2e\,(x,\frac{1}{4},z)$
		$x = 0.277(3)$
	$z = 0.717(1)$	$z = 0.715(2)$
	$U_{\mathrm{iso}} = 0.92(2)$	$U_{\mathrm{iso}} = 1.1(2)$
Occupancy	0.108 (1)	0.108(0)
Te	$2c\,(\frac{1}{4},\frac{1}{4},z)$	$2e\,(x,\frac{1}{4},z)$
		$x = 0.2434(2)$
	$z = 0.28207(5)$	$z = 0.28269(7)$
	$U_{\mathrm{iso}} = 0.94(1)$	$U_{\mathrm{iso}} = 0.75(1)$

of 65(1)% and 35(1)% for the monoclinic and orthorhombic phases, respectively. The details of the refinement of $\mathrm{Fe}_{1.12}\mathrm{Te}$ are compiled in Table II. For $\mathrm{Fe}_{1.13}\mathrm{Te}$, a two-phase refinement of the diffraction pattern taken at 34 K also gives minimum R values for relative fractions of 65% monoclinic and 35% orthorhombic phases. According to Mizuguchi *et al.*, for $\mathrm{Fe}_{1.13}\mathrm{Te}$ the estimated population of the orthorhombic phase at 5 K is 20%–30%, which is close to our results at 10 K.[15]

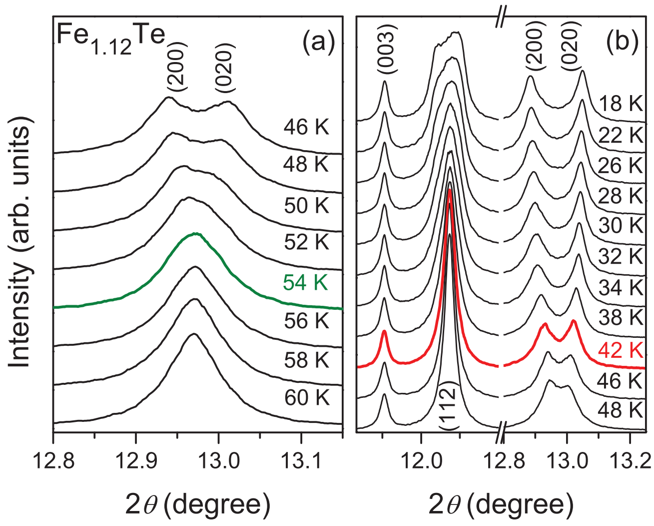

FIG. 8. (Color online) Representative powder XRD patterns of $\mathrm{Fe}_{1.12}\mathrm{Te}$ in the temperature regime 18–60 K. (a) The region of the (200) reflection between 46 and 60 K. (b) The combined region of (112) and (200) reflections between 18 and 48 K. The green and red curves indicate the onset of orthorhombic and monoclinic distortions, respectively.

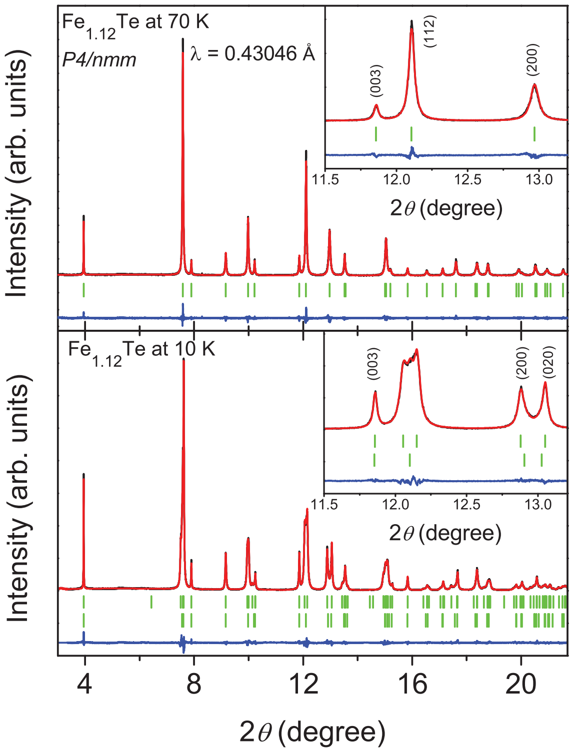

FIG. 9. (Color online) Refined synchrotron powder x-ray diffraction patterns of $\mathrm{Fe}_{1.12}\mathrm{Te}$ at temperatures above (70 K) and below (10 K) the phase transition. At 10 K, the upper and lower Bragg reflections represent monoclinic and orthorhombic structures, respectively.

At a higher Fe content, $y = 0.14$, the broadening of the (200) peak appears at 54 K and visible splitting is monitored at around 50 K (Fig. 10). As expected for an orthorhombic symmetry, the (112) peak does not exhibit broadening or splitting even at the lowest measured temperature. Refined synchrotron powder x-ray diffraction patterns of $\mathrm{Fe}_{1.14}\mathrm{Te}$ at room temperature and 10 K are given in Fig. 11. At 10 K, the XRD pattern of $\mathrm{Fe}_{1.14}\mathrm{Te}$ can be refined assuming a pure orthorhombic phase. Refined parameters of crystal structures at 293 and 10 K are listed in Table III.

We analyzed the full width at half maximum (FWHM) of selected reflections below 70 K for all studied compositions in order to detect broadening and/or splitting of the reflections. The (112) and (200) reflections were selected as identification of symmetry breaking whereas (003) was taken as a reference because its peak shape does not change across the structural transitions. Results are shown in Fig. 12. Here, Δ is given[16] as the sum of the peak FWHM plus the separation of the peak maxima in case of visible splitting, i.e., a value which increases significantly upon peak splitting. In Fig. 12(a), the magnitude of FWHM of both (200) and (112) reflections in $\mathrm{Fe}_{1.11}\mathrm{Te}$ starts to increase almost at the same temperature around 58 K. The difference of ≈2 K between the broadening of (200) and (112) peaks, as mentioned earlier, is difficult to resolve in this analysis. In contrast, the separation between transitions is much more pronounced for the composition $\mathrm{Fe}_{1.12}\mathrm{Te}$ [see Fig. 12(b)]: The (200) reflection

TABLE II. Parameters of crystal structures and refinements, atomic positions, and atomic displacement parameters U_{iso} (in 10^{-2} Å^2) for Fe$_{1.12}$Te in the tetragonal phase at 70 K and in the mixed phase at 10 K.

Temperature	70 K	10 K	10 K
Space group	$P4/nmm$	$P2_1/m$	$Pmmn$
a (Å)	3.81200(5)	3.83845(4)	3.82971(1)
b (Å)	$=a$	3.78807(3)	3.79463 (1)
c (Å)	6.25119(9)	6.25193(5)	6.2521 (1)
β (deg)	90	90.649(1)	90
R_I/R_P	0.013/0.084	0.013/0.054	0.008/0.054
Number of reflections	80	232	133
Refined parameters for profile/crystal structure	22/5	36/11	36/11
Atomic parameters			
Fe1	$2a\ (\frac{3}{4},\frac{1}{4},0)$	$2e\ (x,\frac{1}{4},z)$	$2b\ (\frac{3}{4},\frac{1}{4},z)$
		$x = 0.7378(3)$	
		$z = 0.0019(3)$	$z = 0.0042(7)$
	$U_{\mathrm{iso}} = 0.3418(2)$	$U_{\mathrm{iso}} = 0.2(0)$	$U_{\mathrm{iso}} = 0.2(0)$
Fe2[a]	$2c\ (\frac{1}{4},\frac{1}{4},z)$	$2e\ (x,\frac{1}{4},z)$	$2a\ (\frac{1}{4},\frac{1}{4},z)$
		$x = 0.258(3)$	
	$z = 0.720(1)$	$z = 0.714(2)$	$z = 0.745(3)$
	$U_{\mathrm{iso}} = 0.3(0)$	$U_{\mathrm{iso}} = 0.2(0)$	$U_{\mathrm{iso}} = 0.2(0)$
Te	$2c\ (\frac{1}{4},\frac{1}{4},z)$	$2e\ (x,\frac{1}{4},z)$	$2a\ (\frac{1}{4},\frac{1}{4},z)$
		$x = 0.2432(2)$	
	$z = 0.28319(7)$	$z = 0.2842(1)$	$z = 0.2805(3)$
	$U_{\mathrm{iso}} = 0.3726(1)$	$U_{\mathrm{iso}} = 0.2(0)$	$U_{\mathrm{iso}} = 0.2(0)$

[a] For the refinement involving two phases, the occupancy of the Fe2 site was fixed at $y = 0.12$.

broadens at ≈57 K whereas the value of FWHM of the (112) remains constant until 46 K. These temperatures are in conformity with the specific heat measurements. For the Fe$_{1.13}$Te polycrystalline sample [Fig. 12(c)] a weak broadening in the (112) reflection starts below 40 K, which coincides with the weak first-order phase transition monitored around the same temperature in specific heat. In Fig. 12(d), for $y = 0.14$, no change in the (112) reflections is observed while broadening in (200) reflections is quite obvious because of the transition into orthorhombic symmetry. But the changes in the FWHM values of the (200) reflections for both $y = 0.14$ and $y = 0.15$ (not shown) compositions were observed at

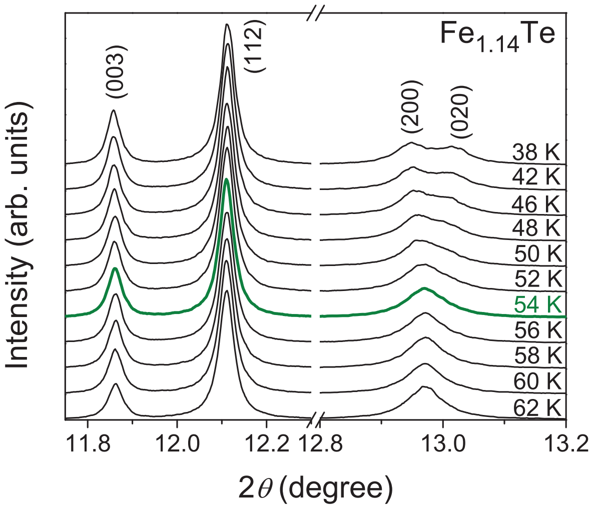

FIG. 10. (Color online) Representative powder XRD patterns of Fe$_{1.14}$Te for the (112) and (200) Bragg reflections in the temperature regime 38–62 K. Broadening of the (200) peak sets in at 54 K (green line).

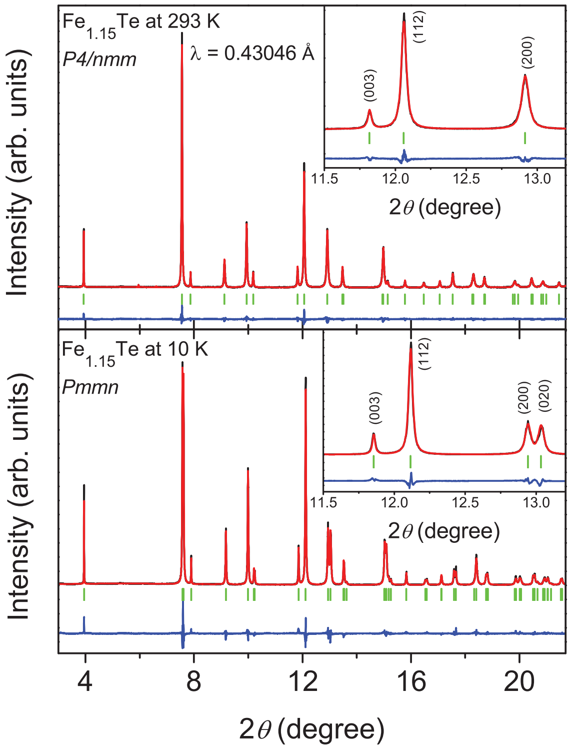

FIG. 11. (Color online) Refined synchrotron powder x-ray diffraction patterns of Fe$_{1.15}$Te at temperatures above (293 K) and below (10 K) the phase transition.

TABLE III. Parameters of crystal structures and refinements, atomic positions, and atomic displacement parameters U_{iso} (in 10^{-2} Å^2) for $Fe_{1.15}Te$ at room temperature and 10 K.

Temperature	293 K	10 K
Space group	$P4/nmm$	$Pmmn$
a (Å)	3.82835(2)	3.81971(3)
b (Å)	$=a$	3.79288(3)
c (Å)	6.27019(4)	6.25288(5)
β (deg)	90	90
R_I/R_P	0.022/0.067	0.021/0.073
Number of reflections	152	133
Refined parameters for profile/crystal structure	22/5	24/7
Atomic parameters		
Fe1	$2a\ (\frac{3}{4},\frac{1}{4},0)$ $U_{iso} = 0.94(1)$	$2b\ (\frac{3}{4},\frac{1}{4},z)$ $z = 0.0020(2)$ $U_{iso} = 0.60(2)$
Fe2	$2c\ (\frac{1}{4},\frac{1}{4},z)$ $z = 0.7175(5)$ $U_{iso} = 0.80(7)$	$2a\ (\frac{1}{4},\frac{1}{4},z)$ $z = 0.7159(8)$ $U_{iso} = 0.5(1)$
Occupancy	0.152 (1)	0.152
Te	$2c\ (\frac{1}{4},\frac{1}{4},z)$ $z = 0.28400(3)$ $U_{iso} = 1.09(1)$	$2a\ (\frac{1}{4},\frac{1}{4},z)$ $z = 0.28490(5)$ $U_{iso} = 0.54(1)$

3–4 K lower than the corresponding antiferromagnetic ordering temperature T_N. The FWHM analyses, in general, show that the onset temperatures of the phase transitions determined by heat capacity measurements are in conformity with the results of synchrotron XRD measurements.

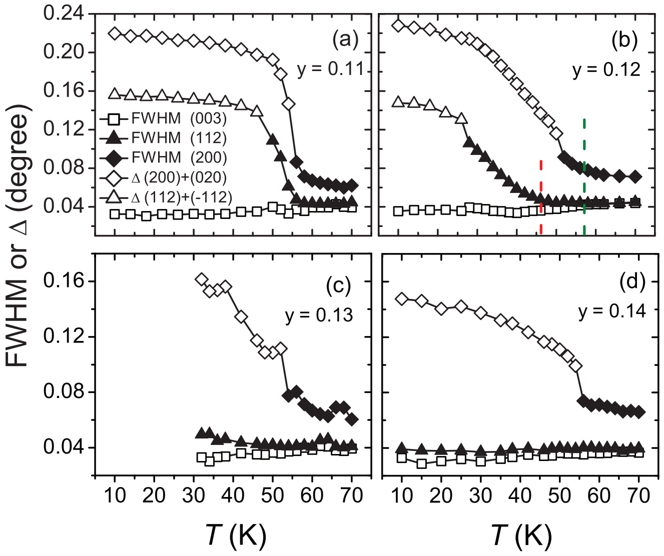

FIG. 12. (Color online) Temperature dependence of powder x-ray diffraction peaks of $Fe_{1+y}Te$, $y = 0.11$–0.14. (a)–(c) The broadening of the reflections (112) and (200) for $0.11 \leqslant y \leqslant 0.13$ demonstrates a monoclinic distortion at low temperatures, whereas in (d) constant values for (112) indicate an orthorhombic low-temperature phase for $y = 0.14$. Dashed lines in (b) were drawn to mark the temperatures at which phase transitions occur in the thermodynamic measurements.

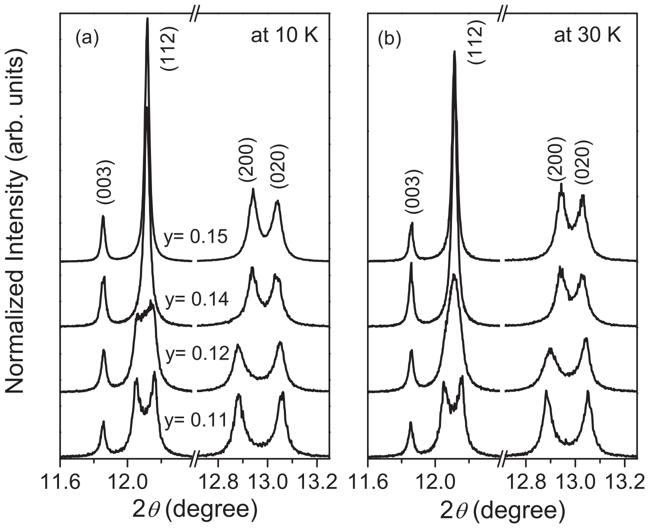

FIG. 13. Representative powder XRD patterns of $Fe_{1+y}Te$, $y = 0.11$–0.15 at (a) 10 K and (b) 30 K. For $y = 0.11$, both (200) and (112) peaks are clearly split at low temperatures, confirming the monoclinic structure. In comparison, the (112) peak of $Fe_{1.12}Te$ is broadened but not as nicely split (specifically at 30 K). This, in combination with the obvious separation of (200) and (020) peaks, is consistent with a mixture of orthorhombic and monoclinic phases at 10 K. For $y \geqslant 0.14$, the narrow (112) peak confirms a pure orthorhombic phase at 30 and 10 K.

In Figs. 13(a) and 13(b), the selected region of XRD patterns for the (112) and (200) Bragg reflections of $Fe_{1+y}Te$, $y = 0.11$–0.15, are given at 10 and 30 K to summarize the low-temperature behaviors of different compositions. Figure 13(b) indicates that the samples $Fe_{1+y}Te$ with $y \geqslant 0.14$ are orthorhombic while $Fe_{1.11}Te$ is in a monoclinic phase already at 30 K. On the other hand, for $Fe_{1.12}Te$ below 30 K the peak broadening of the (112) peak without clear splitting is consistent with a mixture of orthorhombic and monoclinic phases.

Our results on $Fe_{1.12}Te$ are supporting the idea of a two-step evolution of the crystal structure from tetragonal via orthorhombic to monoclinic structures, as suggested by Mizuguchi *et al.*[15] In our previous report on $Fe_{1.13}Te$ single crystals,[14] only one structural phase transition was identified within the magnetically ordered phase, while the present detailed investigations suggest that the low-temperature transition from orthorhombic to monoclinic phase is sluggish and a phase mixture persists even at 10 K for these compositions. The presence of a phase mixture in two samples naturally raises a question about the variation in the Fe composition in each sample, which is about 1%–2% in our sample according to our ICP analysis. Although this can lead to a chemical phase separation, we did not observe any phase separation in the BSE images. Further, the physical property measurements also did not give any evidence for chemical phase separation. By these arguments, we suggest that the crystallographic phase mixture observed at low temperature for $Fe_{1.12}Te$ and $Fe_{1.13}Te$ originates from the slow kinetics of the first-order phase transition from the orthorhombic to monoclinic phase. According to Martinelli *et al.*[24] and our results, for lower Fe content, $y < 0.11$, the phase transition from tetragonal to monoclinic does not need an intermediate phase (orthorhombic) formation. But in the vicinity of a tricritical point on the right-hand side, the intermediate orthorhombic phase slowly transforms towards monoclinic symmetry.

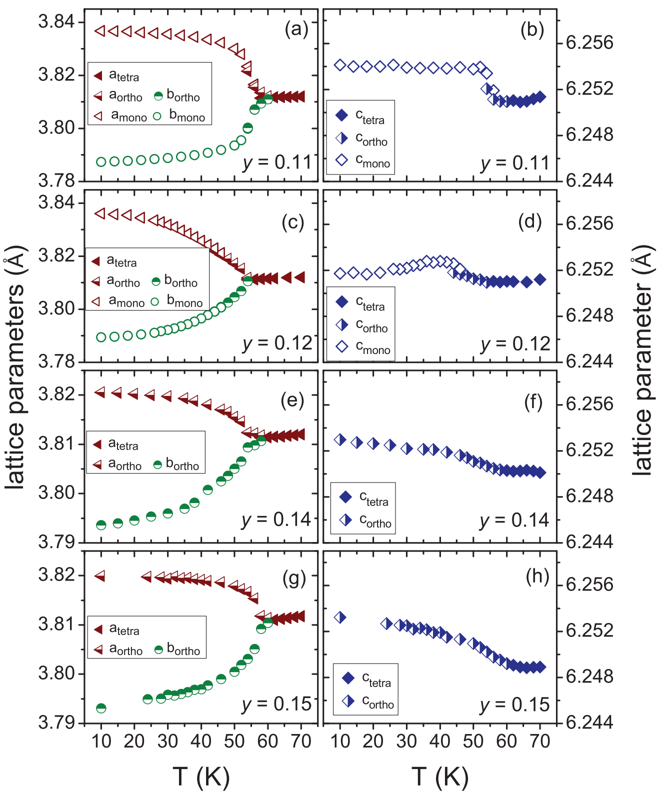

FIG. 14. (Color online) Temperature dependence of lattice parameters a, b, and c at various compositions. (a)–(d) Transition from tetragonal to monoclinic symmetry (with an intermediate orthorhombic phase, represented by half solid symbols) for $y = 0.11$ and 0.12. (e)–(h) Orthorhombic phase transition for $y = 0.14$ and 0.15. Below 46 K, $Fe_{1.12}Te$ consists of a mixture of orthorhombic and monoclinic phases. In (c) and (d), the lattice parameters below 46 K were evaluated assuming a monoclinic structure exclusively.

For a comparison of the metrical changes, the temperature dependence of the lattice parameters obtained from the refinements of several compositions $0.11 \leqslant y \leqslant 0.15$ during the cooling cycle are summarized in Figs. 14(a)–14(h). The splitting of lattice parameter a at around T_N is quite dramatic but remains almost constant throughout the monoclinic phase. In the orthorhombic phase, the difference between lattice parameters a and b is significantly smaller. The difference between the first-order and second-order phase transitions can be clearly seen in the c parameters: For the monoclinic phase transition the increase of the c parameter is sudden at around T_N [Fig. 14(b)], whereas for the orthorhombic phase transition it changes smoothly [see Figs. 14(f) and 14(h)]. The diffraction patterns of $Fe_{1.11}Te$ can be refined as either purely orthorhombic or purely monoclinic phase down to 54 K without a significant difference in the residuals and lattice parameters. In Figs. 14(a) and 14(b), the overlap of lattice parameters for both phases can be seen between 60 and 54 K. Between 46 and 54 K, the lattice parameters of $Fe_{1.12}Te$ were refined as an orthorhombic phase. Below 46 K the lattice parameters were calculated assuming only a monoclinic phase for simplicity. Yet, even when the diffraction pattern was refined, allowing for a mixture of two phases, the lattice parameters of the monoclinic structure did not exhibit a significant difference compared to fitting a purely monoclinic phase. In Figs. 14(c) and 14(d), however, we show the lattice parameters of only the monoclinic phase for clarity. For comparison, also the temperature dependence of the lattice parameters a and b for $Fe_{1.14}Te$ and $Fe_{1.15}Te$ are shown in Figs. 14(e) and 14(g), respectively.

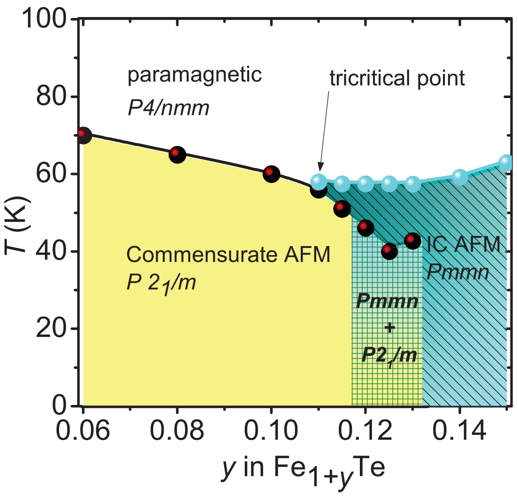

FIG. 15. (Color online) Revised temperature-composition phase diagram of $Fe_{1+y}Te$. AFM and IC AFM stand for antiferromagnetic and incommensurate antiferromagnetic phase, respectively. The data points represent the transition temperatures determined from the specific heat measurements.

On the basis of our results, we propose a revised temperature-composition phase diagram of $Fe_{1+y}Te$ (see Fig. 15). For the lower Fe excess, viz., for $y < 0.11$, the paramagnetic tetragonal phase transforms into a monoclinic commensurate antiferromagnetic phase without an intermediate phase formation while T_N decreases from 69 to 58 K with an increasing Fe amount (as suggested in Ref. 14). A tricritical point is situated close to the composition $y \approx 0.11$ in the phase diagram. At composition, $y = 0.115$, a two-step phase evolution is apparent. At 10 K, for $0.12 \leqslant y \leqslant 0.13$ the materials are composed of a mixture of monoclinic and orthorhombic phases. The temperature difference between these transitions becomes more distinct upon increasing Fe amount. For $y > 0.13$, the phase transition from orthorhombic to monoclinic structure at lower temperature disappears and only a single phase transition is observed. The latter is a second-order phase transition from the tetragonal paramagnetic to orthorhombic incommensurate antiferromagnetic structure, which is in accordance with the neutron scattering experiments.[12]

Now we discuss some open questions concerning the phase diagram of $Fe_{1+y}Te$. The ladder of maximal subgroups for the high symmetry to low symmetry transition is $P4/nmm \rightarrow Pmmn \rightarrow P2_1/m$. A symmetry analysis[25] suggests that these transitions can be continuous. However, the experimentally observed single first-order phase transition for $y < 0.11$ indicates that the transition should be considered as a magnetostructural phase transformation. A theoretical analysis by Paul *et al.* shows[26] several symmetry-allowed magnetoelastic couplings for the $(\pi/2,\pi/2)$ magnetic structure observed for $Fe_{1+y}Te$. The magnetic order parameter couples to the monoclinic component of the uniform lattice strain as well as to the phonon modes (lattice distortions) associated with the wave vectors of high symmetry in the Brillouin zone. Under the assumption that the magnetic mode is the primary order parameter, the magnetoelastic coupling to the fluctuating lattice distortions leads to a weakly first-order transition from the paramagnetic $P4/nmm$ to a bicollinear antiferromagnetic $P2_1/m$ structure for $y < 0.11$.

In the composition range $0.11 \leqslant y \leqslant 0.13$, upon cooling, the system first transforms from a paramagnetic $P4/nmm$ to an incommensurate antiferromagnetic phase with an orthorhombic lattice distortion described by the space group $Pmmn$. The magnitude of the magnetic propagation vector is temperature dependent[12] in the $Pmmn$ phase until the system transforms via a strongly first-order phase transition to a bicollinear antiferromagnetic phase with $P2_1/m$ symmetry. This commensurate-incommensurate magnetic transition appears as a particular type of lock-in transition.[12] $\mathrm{Fe}_{1+y}\mathrm{Te}$ in this composition range shows very strong hysteretic phenomena such as crystallographic phase mixtures and a coexistence of commensurate and incommensurate magnetic domains that resemble the behavior observed in other incommensurately modulated systems (see Ref. 27). This suggests that the transformation of the incommensurate magnetic state in $\mathrm{Fe}_{1+y}\mathrm{Te}$ proceeds via the formation of microstructures on a mesoscopic length scale. Certainly the mechanical incompatibility of the monoclinic commensurate and orthorhombic incommensurate phase plays an important role in this behavior. The variation of the propagation direction with temperature indicates the formation of a soliton lattice.[28] But the usual continuous transformation by a diverging soliton-soliton spacing apparently is intercepted by the first-order jumplike transformation. The phase coexistence of commensurate monoclinic and incommensurate orthorhombic phases in this composition range suggests that the magnetoelastic coupling is responsible for this jumplike behavior. The huge hysteresis effects for the samples in this composition range around the lock-in transition may also be related to pinning by the mixed crystal disorder which can slow down or block the transformation kinetics.[14] Here, either the phase boundaries between commensurate and incommensurate magnetostructural domains or discommensurations as remnants of the incommensurate state may behave as soliton-like entities which are moving in an effective rough potential owing to the statistical distribution of the excess Fe atoms.

For $y > 0.13$, the first-order lock-in transition disappears. This behavior could be understood if the first-order line ends in a critical point, where the commensurate and incommensurate magnetic phases should become indistinguishable from each other, but the neutron diffraction experiments report only an incommensurate magnetic phase for this compositional range.[12,29] Therefore, the ending of the first-order transition line at low temperature is unusual. One possible explanation is by considering the influence of quenched disorder on this first-order transition.[30] At $y > 0.13$, the phase transition may be smeared by quenched disorder. Then, the first-order lock-in line could end at an unusual critical point, where the long-range order is replaced by a thermodynamic state of pinned incommensurate and commensurate magnetic domains.

IV. CONCLUSIONS

We provide a reference data base for cross-comparing different reports on $\mathrm{Fe}_{1+y}\mathrm{Te}$ by conducting low-temperature synchrotron x-ray diffraction experiments, specific heat, magnetic, and resistivity measurements on a single series of chemically well-characterized samples. Based on these data we present a revised phase diagram for $\mathrm{Fe}_{1+y}\mathrm{Te}$. For $y < 0.11$, coinciding magnetic and structural phase transitions occur. For $0.11 < y \leqslant 0.13$ the transition into orthorhombic crystal symmetry is followed by a two-phase region at even lower temperature where also a monoclinic phase is found. In this compositional region, the two phase transitions have both magnetic and structural components. A closer examination suggests a region of orthorhombic crystal symmetry for $y > 0.13$. The coupled magnetic and structural transitions indicate a strong magnetoelastic coupling in this system. However, details of the microscopic couplings and the origin of this complex interplay of magnetic and structural transitions in dependence of the Fe content are yet to be explored.

ACKNOWLEDGMENTS

The authors thank G. Auffermann for chemical analysis, U. Burkhardt for WDX analysis, and W. Schnelle for electrical resistivity measurements. We acknowledge support by A. Fitch and Y. Watier at beamline ID31, ESRF Grenoble, during the experiments based on Proposal No. HS4825. Stimulating discussions with Yu. Grin, U. K. Rößler, and L. H. Tjeng are gratefully acknowledged. The project was supported by DFG SPP 1458. A.A.T. was partly supported by the Mobilitas Grant No. MTT-77 of the ESF.

---

[*] roessler@cpfs.mpg.de

[†] schwarz@cpfs.mpg.de

[1] F.-C. Hsu, J.-Y. Luo, K.-W. Yeh, T.-K. Chen, T.-W. Huang, P. M. Wu, Y.-C. Lee, Y.-L. Huang, Y.-Y. Chu, D.-C. Yan, and M.-K. Wu, Proc. Natl. Acad. Sci. USA **105**, 14262 (2008).

[2] T. M. McQueen, A. J. Williams, P. W. Stephens, J. Tao, Y. Zhu, V. Ksenofontov, F. Casper, C. Felser, and R. J. Cava, Phys. Rev. Lett. **103**, 057002 (2009).

[3] Y. Mizuguchi, F. Tomioka, S. Tsuda, T. Yamaguchi, and Y. Takano, Appl. Phys. Lett. **93**, 152505 (2008).

[4] S. Medvedev, T. M. McQueen, I. A. Troyan, T. Palasyuk, M. I. Eremets, R. J. Cava, S. Naghavi, F. Casper, V. Ksenofontov, G. Wortmann, and C. Felser, Nat. Mater. **8**, 630 (2009).

[5] S. Margadonna, Y. Takabayashi, Y. Ohishi, Y. Mizuguchi, Y. Takano, T. Kagayama, T. Nakagawa, M. Takata, and K. Prassides, Phys. Rev. B **80**, 064506 (2009).

[6] K.-W. Yeh, T.-W. Huang, Y.-L. Huang, T.-K. Chen, F.-C. Hsu, P. M. Wu, Y.-C. Lee, Y.-Y. Chu, C.-L. Chen, J.-Y. Luo, D.-C. Yan, and M.-K. Wu, Europhys. Lett. **84**, 37002 (2008).

[7] M. H. Fang, H. M. Pham, B. Qian, T. J. Liu, E. K. Vehstedt, Y. Liu, L. Spinu, and Z. Q. Mao, Phys. Rev. B **78**, 224503 (2008).

[8] S. Rößler, D. Cherian, S. Harikrishnan, H. L. Bhat, S. Elizabeth, J. A. Mydosh, L. H. Tjeng, F. Steglich, and S. Wirth, Phys. Rev. B **82**, 144523 (2010).

[9] W. Bao, Y. Qiu, Q. Huang, M. A. Green, P. Zajdel, M. R. Fitzsimmons, M. Zhernenkov, S. Chang, M. Fang, B. Qian, E. K. Vehstedt, J. Yang, H. M. Pham, L. Spinu, and Z. Q. Mao, Phys. Rev. Lett. **102**, 247001 (2009).

[10] S. Li, C. de la Cruz, Q. Huang, Y. Chen, J. W. Lynn, J. Hu, Y.-L. Huang, F.-C. Hsu, K.-W. Yeh, M.-K. Wu, and P. Dai, Phys. Rev. B **79**, 054503 (2009).

[11] R. Hu, E. S. Bozin, J. B. Warren, and C. Petrovic, Phys. Rev. B **80**, 214514 (2009).

[12] E. E. Rodriguez, C. Stock, P. Zajdel, K. L. Krycka, C. F. Majkrzak, P. Zavalij, and M. A. Green, Phys. Rev. B **84**, 064403 (2011).

[13] I. A. Zaliznyak, Z. J. Xu, J. S. Wen, J. M. Tranquada, G. D. Gu, V. Solovyov, V. N. Glazkov, A. I. Zheludev, V. O. Garlea, and M. B. Stone, Phys. Rev. B **85**, 085105 (2012).

[14] S. Rößler, D. Cherian, W. Lorenz, M. Doerr, C. Koz, C. Curfs, Yu. Prots, U. K. Rößler, U. Schwarz, S. Elizabeth, and S. Wirth, Phys. Rev. B **84**, 174506 (2011).

[15] Y. Mizuguchi, K. Hamada, K. Goto, H. Takatsu, H. Kadowaki, and O. Miura, Solid State Commun. **152**, 1047 (2012).

[16] C. Koz, S. Rößler, A. A. Tsirlin, D. Kasinathan, C. Börrnert, M. Hanfland, H. Rosner, S. Wirth, and U. Schwarz, Phys. Rev. B **86**, 094505 (2012).

[17] V. Petricek, M. Dusek, and L. Palatinus, JANA2006, The Crystallographic Computing System, Institute of Physics, Praha, Czech Republic, www-xray.fzu.cz/jana.

[18] A. March, Z. Kristallogr. **81**, 285 (1932).

[19] W. A. Dollase, J. Appl. Crystallogr. **19**, 267 (1986).

[20] S. Chiba, J. Phys. Soc. Jpn. **10**, 837 (1955).

[21] H. Ipser, K. L. Komarek, and H. Mikler, Monatsh. Chem. **105**, 1322 (1974).

[22] H. Okamoto and L. E. Tanner, in *Binary Alloy Phase Diagrams*, edited by T. B. Massalski (ASM International, Cleveland, OH, 1990), Vol. 2, p. 1781.

[23] L. Zhang, D. J. Singh, and M. H. Du, Phy. Rev. B **79**, 012506 (2009).

[24] A. Martinelli, A. Palenzona, M. Tropeano, C. Ferdeghini, M. Putti, M. R. Cimberle, T. D. Nguyen, M. Affronte, and C. Ritter, Phys. Rev. B **81**, 094115 (2010).

[25] A. Martinelli, J. Phys.: Condens. Matter **25**, 125703 (2013).

[26] I. Paul, A. Cano, and K. Sengupta, Phys. Rev. B **83**, 115109 (2011).

[27] B. A. Strukov, Phase Transitions **15**, 143 (1989) and references therein.

[28] D. Parshall, G. Chen, L. Pintschovius, D. Lamago, Th. Wolf, L. Radzihovsky, and D. Reznik, Phys. Rev. B **85**, 140515(R) (2012).

[29] C. Stock, E. E. Rodriguez, M. A. Green, P. Zavalij, and J. A. Rodriguez-Rivera, Phys. Rev. B **84**, 045124 (2011).

[30] Y. Imry and M. Wortis, Phys. Rev. B **19**, 3580 (1979).